

Equivalent Circuit Representation of a Parallel Plate Waveguide Fed Connected Array

Coco Martin, C.M.; Cavallo, Daniele

10.1109/TAP.2024.3508061

Publication date

Document Version Final published version

Published in

IEEE Transactions on Antennas and Propagation

Citation (APA)
Coco Martin, C. M., & Cavallo, D. (2024). Equivalent Circuit Representation of a Parallel Plate Waveguide Fed Connected Array. *IEEE Transactions on Antennas and Propagation*, 73(3), 1496 - 1504. https://doi.org/10.1109/TAP.2024.3508061

Important note

To cite this publication, please use the final published version (if applicable). Please check the document version above.

Other than for strictly personal use, it is not permitted to download, forward or distribute the text or part of it, without the consent of the author(s) and/or copyright holder(s), unless the work is under an open content license such as Creative Commons.

Takedown policy

Please contact us and provide details if you believe this document breaches copyrights. We will remove access to the work immediately and investigate your claim.

Green Open Access added to TU Delft Institutional Repository 'You share, we take care!' - Taverne project

https://www.openaccess.nl/en/you-share-we-take-care

Otherwise as indicated in the copyright section: the publisher is the copyright holder of this work and the author uses the Dutch legislation to make this work public.

Equivalent Circuit Representation of a Parallel Plate Waveguide Fed Connected Array

Caspar M. Coco Martin[®], Graduate Student Member, IEEE, and Daniele Cavallo[®], Senior Member, IEEE

Abstract—We present an analytical model to describe arrays of connected slots fed by parallel plate waveguides (PPWs). Connected slot arrays are planar ultrawideband arrays with wide scanning capability. PPW feeds can be used to reduce the complexity of the unit cell design. However, existing analytical expressions of the active input impedance of the array cannot account for the presence of PPWs. Here, we develop a new model that includes PPW structures in the stratification, enabling the optimization of the design together with the feed. An equivalent circuit of the unit cell is derived, where the PPW sections are represented in terms of equivalent transmission lines for each Floquet mode. Closed-form expressions are also derived for the capacitance associated with step discontinuities of the PPW and the inductance associated with the feed. Full-wave simulations are used to validate the model.

Index Terms—Artificial dielectrics, connected arrays, parallel plate waveguide (PPW), spectral domain method, wideband arrays.

I. INTRODUCTION

ODERN radar and telecommunication systems can benefit from wideband antenna arrays, to combine multiple functions in a single aperture, and thus reduce the total volume and weight of the system. The most popular solutions for wideband antenna arrays belong to two families: connected or tightly coupled arrays [1], [2] and tapered slot arrays [3], [4]. The latter have typically electrically large heights, which makes them unsuitable for applications that require low-profile arrays. On the contrary, connected arrays can obtain comparable performance as tapered slot arrays in terms of bandwidth, but with a lower vertical profile.

To radiate in a single direction, connected array designs include a backing reflector, which limits the operational bandwidth. Artificial dielectric layers (ADLs) have been proposed in [5], [6], and [7] to overcome the frequency dependence of the reflector and enlarge the bandwidth. These are periodic arrangements of subwavelength metal patches to synthesize a desired effective refractive index. Unlike conventional dielectric slabs, ADLs are highly anisotropic and do not support

Received 28 June 2024; revised 1 November 2024; accepted 19 November 2024. Date of publication 9 December 2024; date of current version 5 March 2025. This work was supported in part by Thales SA and in part by Thales DMS France SAS through the Project "Wideband Wide-Scanning Arrays with Improved Cross-Polarization Purity". (Corresponding author: Caspar M. Coco Martin.)

The authors are with the Microelectronics Department, Faculty of Electrical Engineering, Mathematics and Computer Science (EEMCS), Delft University of Technology, 2628 CD Delft, The Netherlands (e-mail: c.m.cocomartin@tudelft.nl; d.cavallo@tudelft.nl).

Digital Object Identifier 10.1109/TAP.2024.3508061

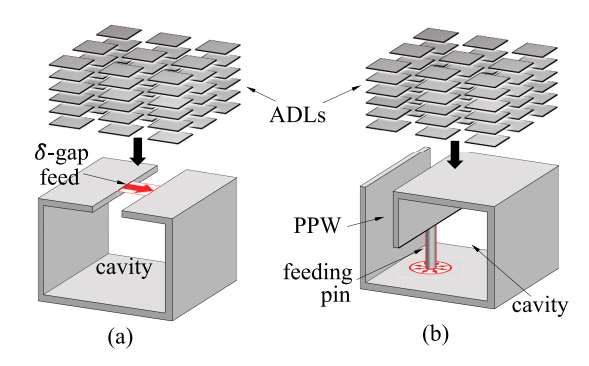


Fig. 1. Schematic of a cavity-backed connected array unit cell, loaded with ADLs. (a) Delta-gap feed on the slot plane and (b) feeding structure consisting of a PPW section beside the cavity excited with a pin.

surface waves, allowing for wide scanning with stable input impedance.

Another benefit of connected arrays is that analytical solutions are available for the active input impedance of the array in the presence of ADLs [6], [8]. These solutions allow simulation of the unit cell with negligible computational resources, enabling the optimization of the performance in the design phase. The unit cell consists of a cavity-backed connected slot loaded with ADLs [Fig. 1(a)]. The feed is represented by a delta-gap source located at the slot plane. Such a feed would require an additional coaxial transition to transfer the input below the ground plane. The design of this transition is not trivial, as it degrades the impedance matching and requires large aspect ratio vias [7].

An alternative feed concept, consisting of a parallel-plate waveguide (PPW), was proposed in [9], and was shown to simplify the feeding structure of connected slot arrays. The radiating slot is fed by a vertical PPW and the cavity is folded, to be positioned next to the PPW, allowing a single vertical pin to feed the structure [Fig. 1(b)]. The resulting unit cell has two main advantages: the PPW can implement a part of the impedance transformer, reducing the number of metal layers required for the ADLs; the feed is now already located at the ground plane, and thus, no additional transition is required.

Despite the advantages of the PPW feed, the existing analytical models of connected arrays [6] do not include the PPW, which is an integral part of the unit cell design. The goal of this work is to derive a new model that rigorously accounts for the effects of the PPWs. An analysis of periodic PPWs under a generic dielectric stratification was presented in

0018-926X © 2024 IEEE. Personal use is permitted, but republication/redistribution requires IEEE permission. See https://www.ieee.org/publications/rights/index.html for more information.

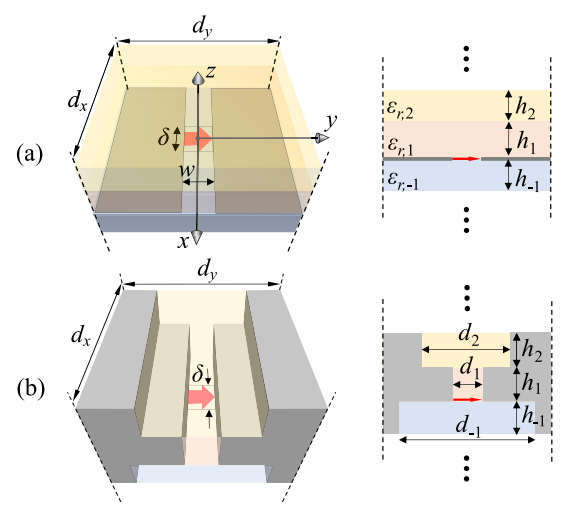


Fig. 2. (a) Unit cell of a connected slot in a stratified medium, periodically fed by a delta-gap source and (b) connected slot in a PPW stratified medium, with characteristic geometrical parameters.

TABLE I
COMPARISON WITH PREVIOUS WORKS
Model includes

	PPW modes	Feed reactance	Eq. Circuit
[6]	N.A.	Yes	Yes
[10], [11]	TE and TM	No	No
This work	Only TEM	Yes	Yes

[10] and [11], based on a mode matching method, assuming a plane-wave-like incident field in the PPW. However, this approach does not consider the dimension of the feed in a periodic array and it does not lend itself to a simple equivalent circuit representation.

Here, a different approach is proposed, based on the Floquet expansion, where we assume that only transverse electromagnetic (TEM) modes can propagate in the PPW (see Table I). The advantage of our formulation is that it can provide an equivalent circuit of the unit cell, which gives physical insight and aids the design of the array. In the equivalent circuit, the PPW sections are represented in terms of equivalent transmission lines for each Floquet mode. Closed-form expressions are also found for the capacitance associated with a step discontinuity of the PPW and the inductance associated with the feed dimension. Full-wave simulations based on commercial electromagnetic solvers are used to validate the model.

II. GEOMETRY OF THE PROBLEM AND SOLUTION

A typical connected array unit cell is depicted in Fig. 2(a) and consists of an x-oriented connected slot element, with periods d_x and d_y along x and y, respectively. The slot width is indicated by w, and δ refers to the delta-gap feed size. Both w and δ are assumed to be small compared with the wavelength. The slot is located within a general stratified dielectric medium. A different type of unit cell is considered in this article and is drawn in Fig. 2(b). This structure consists of a slot embedded in a layered medium made by PPWs with a different widths d_i and heights h_i , where i is chosen as a positive index to indicate the layers above the feed and negative for the layers below. The goal is to find an expression of the active input impedance for general structures, that might include combinations of PPW sections and dielectric slabs.

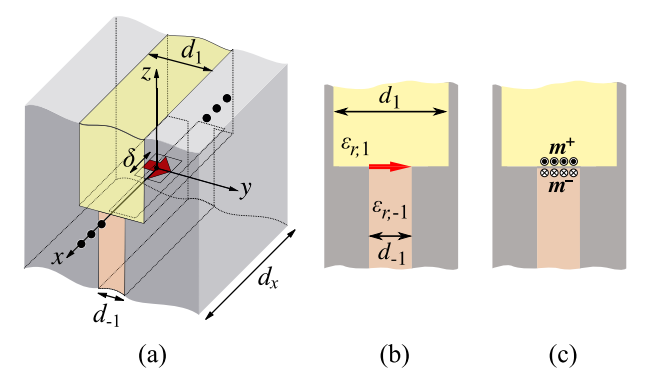


Fig. 3. Unit cell of a connected PPW array, with delta-gap feed at interface between two semi-infinite PPWs with plate distance d_{-1} and d_1 . (a) 3-D view and (b) side view of the problem and (c) application of the equivalence theorem, with a perfect electric conductor sheet placed at the feed plane, and equal and opposite equivalent magnetic currents above and below the sheet.

A. Integral Equation in the Space Domain and Assumption for the Magnetic Current Distribution

As the starting point, we first consider the simple case of two PPWs infinitely extended in the vertical direction, as shown in Fig. 3(a). The PPWs for z > 0 and z < 0 are characterized by plate spacing d_1 and d_{-1} , respectively, and are fed at the discontinuity by delta-gap feeds with size δ and width d_{-1} (assuming $d_{-1} < d_1$), periodically spaced by d_x . The upper and lower PPWs are filled with materials of relative permittivity $\varepsilon_{r,1}$ and $\varepsilon_{r,-1}$, respectively, as shown in the side view of the structure in Fig. 3(b).

By applying the equivalence theorem, we define the equivalent magnetic currents on the aperture at the PPW discontinuity, as shown in Fig. 3(c). The magnetic currents m^+ and m^- are located above and below a thin perfect electric conductor sheet, and they are equal and opposite to satisfy the continuity of the electric field at the feed plane ($m = m^+ = -m^-$). For electrically narrow PPWs, the magnetic currents are also assumed to be oriented along x, i.e., $m = m_x \hat{x}$.

Imposing the continuity of the magnetic field on the feed plane, one can write the magnetic field integral equation (MFIE) as follows:

$$\int_{-\infty}^{\infty} \int_{-\infty}^{\infty} g_{xx}(x - x', y - y') m_x(x', y') dx' dy' = -j_i(x, y)$$

$$\tag{1}$$

where g_{xx} is the xx component of Green's function relating magnetic field to magnetic sources and can be written as the sum of Green's functions of the upper and lower PPWs

$$g_{xx}(x, y) = g_{xx,1}(x, y) + g_{xx,-1}(x, y).$$
 (2)

The term $j_i(x, y)$ is the incident current associated with the periodic feeds, given by

$$j_i(x, y) = \sum_{n_x = -\infty}^{\infty} \frac{I_0}{\delta} \text{rect}_{\delta}(x - n_x d_x) e^{-jk_{x0}n_x d_x} \text{rect}_{d_{-1}}(y)$$
 (3)

where I_0 is the amplitude of the current source and the function $rect_a(x)$ is defined as follows:

$$rect_a(x) = \begin{cases} 1, & \text{for } |x| \le a/2\\ 0, & \text{otherwise.} \end{cases}$$
 (4)

The exponent term in (3) accounts for the linear phase shift to scan in the xz plane, where $k_{x0} = k_0 \sin \theta$, and k_0 and θ are the wavenumber and scan angle in free space, respectively. According to the Snell law, $k_0 \sin \theta = k_i \sin \theta_i$, with $i = \pm 1$, where k_i and θ_i are the wavenumber and the scan angle in the media filling the PPWs.

By applying the separation of variables, one can write the surface magnetic current as follows:

$$m_x(x', y') = v(x')m_t(y')$$
 (5)

where the transverse distribution is assumed to be uniform, corresponding to the TEM mode in a PPW

$$m_t(y') = \frac{1}{d_{-1}} \operatorname{rect}_{d_{-1}}(y')$$
 (6)

while the longitudinal distribution v(x') is the unknown of the integral equation. Due to the periodicity along x, this distribution satisfies the condition $v(x' + n_x d_x) = v(x')e^{-jk_{x0}n_x d_x}$.

B. Integral Equation in the Spectral Domain

Following the steps similar to [12], the integral equation in (1) can be written in the spectral domain. By applying the Poisson formula to account for the periodicity along x and the presence of perfectly electric conductor (PEC) walls along y, the spectral integrals are converted into discrete Floquet sums

$$\frac{1}{d_{x}} \sum_{m_{x}=-\infty}^{\infty} \sum_{m_{y}=-\infty}^{\infty} \left(\frac{G_{xx,1}(k_{xm}, k_{ym,1}) M_{t}(k_{ym,1}) e^{-jk_{ym,1}y}}{d_{1}} + \frac{G_{xx,-1}(k_{xm}, k_{ym,-1}) M_{t}(k_{ym,-1}) e^{-jk_{ym,-1}y}}{d_{-1}} \right)$$

$$\times V(k_{xm})e^{-jk_{xm}x}$$

$$= \frac{1}{d_x} \sum_{m=-\infty}^{\infty} \operatorname{sinc}\left(\frac{k_{xm}\delta}{2}\right) e^{-jk_{xm}x} \operatorname{rect}_{d_{-1}}(y) \tag{7}$$

where $k_{xm} = k_{x0} - 2\pi m_x/d_x$ and

$$M_t(k_{ym,i}) = \operatorname{sinc}\left(\frac{k_{ym,i}d_{-1}}{2}\right) \tag{8}$$

is the Fourier transform of the transverse distribution in (6), with $k_{ym,i} = -2\pi m_y/d_i$ and $i = \pm 1$ for the regions z > 0 and z < 0, respectively. The functions denoted with uppercase symbols $G_{xx,i}(k_x, k_y)$ and $V(k_x)$ refer to the Fourier transforms of their spatial counterparts $g_{xx,i}(x, y)$, and v(x), respectively.

To solve the equation for $V(k_{xm})$, we apply the Galerkin projection on the test function defined in (6) and (8). This is equivalent to integrating both left- and right-hand sides of (7) over the slot width $\int_{-d_{-1}/2}^{d_{-1}/2} (\cdot) dy$ and dividing by the width d_{-1} . After some algebraic steps, this operation results in

$$\frac{1}{d_x} \sum_{m_x = -\infty}^{\infty} \left[D_1(k_{xm}) + D_{-1}(k_{xm}) \right] V(k_{xm}) e^{-jk_{xm}x}$$

$$= \frac{1}{d_x} \sum_{m_x = -\infty}^{\infty} \operatorname{sinc}\left(\frac{k_{xm}\delta}{2}\right) e^{-jk_{xm}x} \tag{9}$$

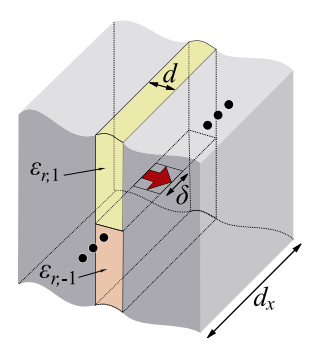


Fig. 4. 3-D view of connected PPW unit cell with periodic feeds.

where we defined

$$D_i(k_{xm}) = \frac{1}{d_i} \sum_{m_y = -\infty}^{\infty} G_{xx,i}(k_{xm}, k_{ym,i}) \operatorname{sinc}^2\left(\frac{k_{ym,i}d_{-1}}{2}\right).$$
(10)

C. Active Input Impedance

Because (9) is valid for every x, the terms in the sums can be equated, and one can solve for the discrete voltage spectrum

$$V(k_{xm}) = -\frac{I_0 \text{sinc}(\frac{k_{xm}\delta}{2})}{D_1(k_{xm}) + D_{-1}(k_{xm})}.$$
 (11)

The active input impedance of the array can be defined as the ratio of the average voltage and the current over the feeding gap. By applying the discrete inverse Fourier transform to (11) and averaging it over the feeding gap, we can obtain the input voltage, which is divided by the impressed current I_0 to give the active input impedance as follows:

$$Z_{\rm in} = -\frac{1}{d_x} \sum_{m_x = -\infty}^{\infty} \frac{\sin^2\left(\frac{k_{xm}\delta}{2}\right)}{D_1(k_{xm}) + D_{-1}(k_{xm})}.$$
 (12)

The expression in (12) is valid for uniform voltage on the feeding gap. This is the case for broadside and E-plane scanning, even if the size of the feed δ is not much smaller than the period d_x . However, when scanning to large angles in the H-plane and for large values of δ , the voltage can vary over the feeding gap. For these cases, the correction method described in the Appendix can be used to account for the voltage variations over the gap, yielding improved accuracy for the H-plane scanning.

III. NONSTEPPED PPW

A special case of the previously described geometry is when the two PPWs have equal plate spacing $d_1 = d_{-1} = d$, as shown in Fig. 4. The function D_i in (10) simplifies as follows:

$$D_{i}(k_{xm}) = \frac{1}{d} \sum_{m_{y}=-\infty}^{\infty} G_{xx,i} \left(k_{xm}, \frac{-2\pi m_{y}}{d} \right) \operatorname{sinc}^{2} (\pi m_{y})$$

$$= \frac{1}{d} G_{xx,i}(k_{xm}, 0)$$
(13)

where we used the identity

$$\operatorname{sinc}(\pi m_y) = \begin{cases} 1, & \text{for } m_y = 0\\ 0, & \text{for } m_y \neq 0. \end{cases}$$
 (14)

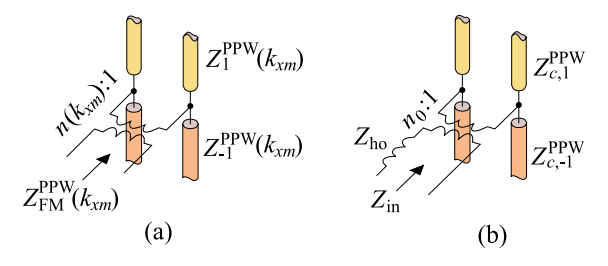


Fig. 5. (a) Equivalent transmission line representation for each Floquet mode and (b) equivalent circuit for the total input impedance with the fundamental Floquet mode represented as transmission lines and the higher order modes represented as an equivalent inductance.

By assuming that the PPW is infinitely extended and filled with a homogeneous material, we can substitute the spectral Green's function for an infinite homogeneous dielectric halfspace

$$G_{xx,i}^{\text{hs}}(k_x, k_y) = -\frac{k_i^2 - k_x^2}{k_0 \zeta_0 \sqrt{k_i^2 - k_x^2 - k_y^2}}$$
(15)

where $k_i = k_0 \sqrt{\varepsilon_{r,i}}$ and ζ_0 is the free-space wave impedance. By replacing (15) in (13), we obtain

$$D_i(k_{xm}) = -\frac{1}{d} \frac{\sqrt{k_i^2 - k_{xm}^2}}{k_0 \zeta_0}.$$
 (16)

By substituting (16) into (12), one can find the active input impedance of a periodically fed PPW

$$Z_{\text{in}}^{\text{PPW}} = \sum_{m_x = -\infty}^{\infty} \frac{\sin^2(k_{xm}\delta/2)}{\frac{d_x}{d} \frac{\sqrt{k_1^2 - k_{xm}^2}}{k_0 \zeta_0} + \frac{d_x}{d} \frac{\sqrt{k_{-1}^2 - k_{xm}^2}}{k_0 \zeta_0}}$$
$$= \sum_{m_x = -\infty}^{\infty} Z_{\text{FM}}^{\text{PPW}}(k_{xm})$$
(17)

where each of the terms of the sum, indicated as $Z_{\text{FM}}^{\text{PPW}}(k_{xm})$, can be interpreted as the impedance of the m_x th Floquet mode.

A. Equivalent Circuit of Nonstepped Connected PPW

It is convenient to represent the impedance in (17) in terms of an equivalent circuit model. A possible representation can be obtained for each Floquet mode by noting that $Z_{\rm FM}^{\rm PPW}$ is the parallel between two infinite transmission lines with characteristic impedance

$$Z_i^{\text{PPW}}(k_{xm}) = \frac{d\zeta_0}{d_x \sqrt{\varepsilon_{r,i} - k_{xm}^2 / k_0^2}}$$
(18)

with $i = \pm 1$, connected to a transformer with turn ratio $n(k_{xm}) = \text{sinc}(k_{xm}\delta/2)$. The resulting circuit is shown in Fig. 5(a) and will be later used to represent the higher order Floquet modes in more general stratification.

Another convenient representation can be made for the total input impedance in (17), by splitting the impedance in the fundamental mode ($m_x = 0$) and higher order modes ($m_x \neq 0$)

$$Z_{\text{in}}^{\text{PPW}} = \frac{\text{sinc}^2(k_{x0}\delta/2)}{1/Z_{c,1}^{\text{PPW}} + 1/Z_{c,-1}^{\text{PPW}}} + Z_{\text{ho}}$$
(19)

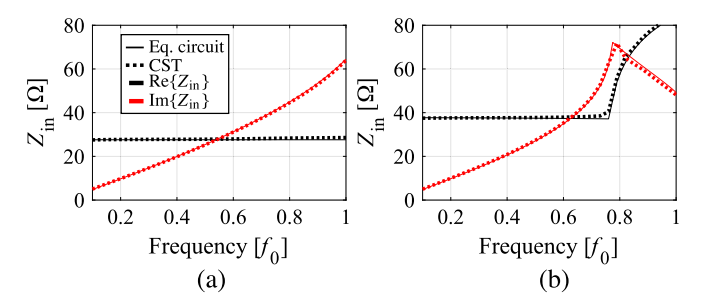


Fig. 6. Active input impedance of periodic PPW for (a) broadside and (b) scanning to $\theta=60^\circ$. Unit cell parameters: $d_x=0.5\lambda_0$, $d_{\text{PPW}}=d_{\text{down}}=0.1\lambda_0$, $\delta=0.1\lambda_0$, $\varepsilon_{r,-1}=3$, and $\varepsilon_{r,1}=1$.

where the fundamental mode is the parallel of two infinite transmission lines with characteristic impedance $Z_{c,i}^{PPW} = Z_i^{PPW}(k_{x0})$ from (18), representing the propagation in the PPW [see Fig. 5(b)]. The multiplying constant is expressed as a transformer with turn ratio n_0 :1, with $n_0 = \text{sinc}(k_{x0}\delta/2)$. For $k_{x0} = 0$, the turn ratio n_0 becomes 1, and $Z_{c,i}^{PPW}$ reduces to the well-known equation for the characteristic impedance of the TEM mode in a PPW [13].

For a well-sampled array, the higher order Floquet modes do not propagate, thus the term Z_{ho} is purely reactive and can be associated with the inductance of the feed

$$Z_{\text{ho}} = j\omega\mu_0 \frac{d}{d_x} \sum_{m_x \neq 0} \frac{\text{sinc}^2(k_{xm}\delta/2)}{\sqrt{k_{xm}^2 - k_1^2} + \sqrt{k_{xm}^2 - k_{-1}^2}}$$
(20)

where ω is the angular frequency and μ_0 is the free space permeability.

It can be noted that the circuit in Fig. 5 is also valid for scanning since all circuit components depend on the scan angle θ through the Floquet wavenumbers k_{xm} .

B. Validation of Nonstepped Periodic PPW Model

As an example, we consider a PPW geometry with $d_x = 0.5\lambda_0$, $d = 0.1\lambda_0$, $\delta = 0.1\lambda_0$, $\varepsilon_{r,-1} = 3$, and $\varepsilon_{r,1} = 1$, where λ_0 is the wavelength at the frequency f_0 . The analytical input impedance is compared with simulations in CST Microwave Studio in Fig. 6, for broadside and scanning to 60° in the upper PPW. There is a good correspondence between the two methods. If only the fundamental Floquet mode propagates, the real part of the input impedance is frequency independent, as it represents the characteristic impedance of the PPW lines. The input reactance can be associated with the inductance of the feed. When scanning, the real part of the active impedance is constant until $0.75\,f_0$, and then, the first higher order Floquet mode enters the visible region, as expected from the condition $k_i^2 - k_{xm}^2 > 0$, creating a discontinuous derivative in the curve.

IV. STEPPED PPW

Building upon the structure presented in Section III, a more general structure that can be studied is the case, where the two PPWs have different plate spacing $d_{-1} \neq d_1$ [see Fig. 7(a)].

Because of the step discontinuity, while the simplification in (16) can be used for the lower PPW, the more general expression in (10) must be used for the upper PPW. The

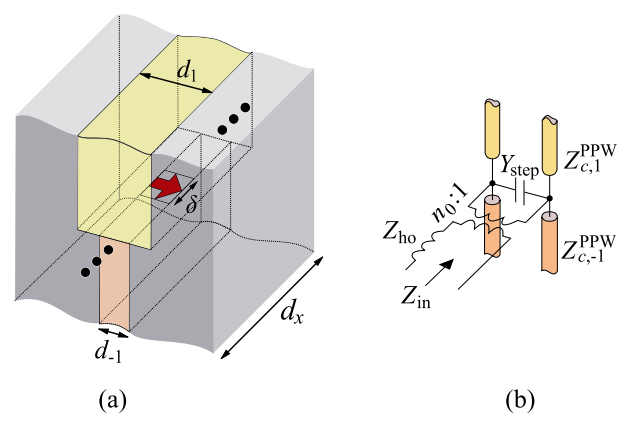


Fig. 7. Connected PPW with step discontinuity and periodic feeds. (a) 3-D view and (b) equivalent circuit.

higher order Floquet modes $k_{ym,1} = -2\pi m_y/d_1$, for $m_y \neq 0$, contribute to the reactive field, representing the fringing field at the discontinuity.

A. Equivalent Step Capacitance

The reactance due to the fringing field at the PPW step can be modeled as a shunt capacitance [14] in the equivalent circuit for $m_x = 0$. If we split the expression in (10) into the fundamental $(m_y = 0)$ and higher order modes $(m_y \neq 0)$, we can identify the parallel of two transmission lines representing the propagation in the PPWs, with characteristic impedance described by (18), and a reactive admittance associated with the higher order modes

$$Y_{\text{step}} = -\frac{d_x}{d_1} \sum_{m_y \neq 0} G_{xx,1}^{\text{hs}} \left(k_{x0}, \frac{-2\pi m_y}{d_1} \right) \operatorname{sinc}^2 \left(\frac{\pi m_y d_{-1}}{d_1} \right).$$
(21)

Substituting (15) into (21), we can write

$$Y_{\text{step}} = j\omega\varepsilon_0\varepsilon_{r,1}\frac{d_x}{d_1}\sum_{m_y\neq 0} \frac{\left(1 - k_{x0}^2/k_1^2\right)\operatorname{sinc}^2\left(\frac{\pi m_y d_{-1}}{d_1}\right)}{\sqrt{\left(2\pi m_y/d_1\right)^2 - k_1^2 - k_{x0}^2}} \tag{22}$$

where ε_0 is the free-space permittivity. In the equation, the factor $j\omega\varepsilon_0\varepsilon_{r,1}$ can be recognized as typical of a capacitance. A schematic drawing of the equivalent circuit is given in Fig. 7(b). For brevity, the circuit for each Floquet mode is omitted, and all higher order mode circuits are summed together in the feed inductance, which can be written in the most general form as follows:

$$Z_{\text{ho}} = -\frac{1}{d_x} \sum_{m_x \neq 0} \frac{\sin^2(k_{xm}\delta/2)}{D_1(k_{xm}) + D_{-1}(k_{xm})}.$$
 (23)

B. Noncentered PPWs

The axes of the PPWs do not necessarily have to be aligned. For example, a structure as shown in Fig. 8 could be of interest, specifically for the PPW-fed connected array unit cell. We indicate with s the shift in the y-direction of the narrower PPW w.r.t. the center of the wider PPW.

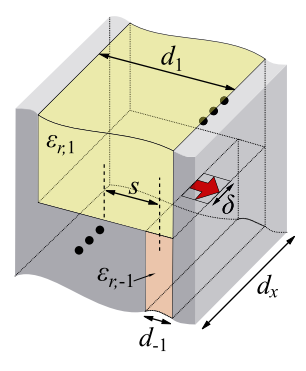


Fig. 8. Schematic of unit cell with noncentered PPWs.

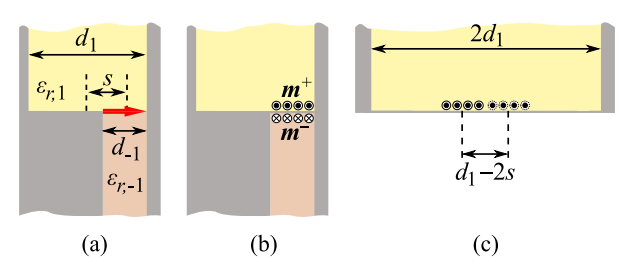


Fig. 9. (a) Side view of nonaligned stepped PPW, periodically fed with delta-gap generator. (b) Equivalence theorem: PEC sheet placed in the feed, and equal and opposite magnetic currents above and below the sheet. (c) Image theorem is applied once to make the upper PPW symmetric.

The side view of the structure is shown in Fig. 9(a), while the application of the equivalence principle is depicted in Fig. 9(b), highlighting a nonsymmetric unit cell for the upper PPW. By applying the image theorem for one of the two walls of the larger PPW, a unit cell with a period of $2d_1$ is defined, as shown in Fig. 9(c), which includes the original current distribution and the image. Thus, to take into account the shift between the PPWs, an extra term must be considered that represents a phase-shifted copy of the feed in the spectral domain. After some algebraic steps, one can derive the correction term that should be multiplied inside the Floquet sum of (21) and (22)

$$C(m_y) = \frac{1 + e^{-j\pi m_y (d_1 - 2s)/d_1}}{2}.$$
 (24)

In this equation, the period in y is effectively doubled, meaning that the step capacitance is modified as follows:

$$Y_{\text{step}} = -\frac{d_x}{d_1} \sum_{m_y \neq 0} G_{xx,1}^{\text{hs}} \left(k_{x0}, \frac{-\pi m_y}{d_1} \right) \operatorname{sinc}^2 \left(\frac{\pi m_y d_{-1}}{2d_1} \right) C(m_y).$$
(25)

C. Validation of Stepped PPW Model

For validation, full-wave simulations are made of a stepped PPW, with and without shift. The resulting input impedance is shown in Fig. 10. The solid curves are from the equivalent circuit, while the dotted curves are the CST simulation result. A good correspondence can be observed for two considered cases, where no shift is present (s = 0) in Fig. 10(a), and with shift $s = (d_1 - d_{-1})/2$ in Fig. 10(b). Both figures refer to a scan angle $\theta = 60^{\circ}$. It can be noted that a resonance corresponding to a zero of the input resistance occurs around 0.55 f_0 in the case with the shift, while it is not present in the

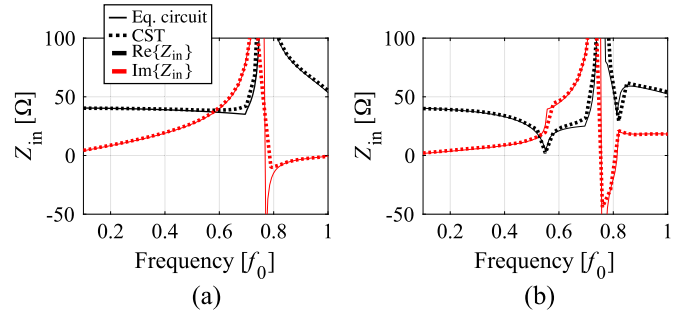


Fig. 10. Active input impedance of stepped PPW with $d_x = 0.5\lambda_0$, $d_1 = 0.5\lambda_0$, $d_{-1} = 0.1\lambda_0$, $\varepsilon_{r,1} = 4$, $\varepsilon_{r,-1} = 3$, and $\delta = 0.1\lambda_0$ for scanning to $\theta = 60^\circ$, for different shifts. (a) s = 0. (b) $s = (d_1 - d_{-1})/2$.

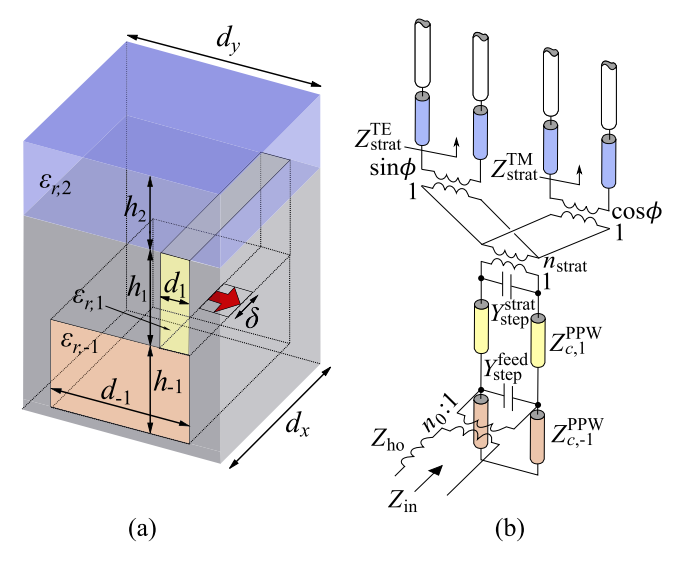


Fig. 11. (a) Schematic of the full structure to analyze, including an arbitrary horizontal stratification and (b) equivalent circuit representation.

absence of the shift. This highlights the importance of properly accounting for the shift in the estimation of the impedance.

V. ANALYSIS OF CONNECTED PPW ARRAY UNIT CELLS

With the spectral Green's function of the PPW defined, and the introduced step capacitance and feed inductance formulas, one can derive an expression for the active input impedance of a more general PPW-fed connected slot array unit cell, such as the one depicted in Fig. 11(a). For example, we can consider a unit cell consisting of a feed with width δ backed by a noncentered dielectric-filled cavity with relative permittivity $\varepsilon_{r,-1}$ and height h_{-1} , modeled as a shorted PPW section with plate spacing d_{-1} . Above the feed, there is a PPW with plate spacing d_1 and length h_1 , filled with a material of permittivity $\varepsilon_{r,1}$. The open end of this PPW line is loaded with a generic stratification that might include real or artificial dielectric slabs. In the figure, as an example, a dielectric slab is considered, with height h_2 and relative permittivity $\varepsilon_{r,2}$.

To find the input impedance of this unit cell, it is convenient to first rewrite (12) in a more general form that depends on the input admittances of the stratification above and below the feed plane

$$Z_{\rm in} = \sum_{m=-\infty}^{\infty} \frac{{\rm sinc}^2(k_{xm}\delta/2)}{Y_{\rm up}(k_{xm}) + Y_{\rm down}(k_{xm})}.$$
 (26)

We can then derive the expressions for these two admittances.

A. Medium Below the Feed

We can define the input admittance looking into the cavity $Y_{\text{down}}(k_x)$, by defining Green's function of the cavity, given by

$$G_{xx}^{\text{cav}}\left(k_{xm}, \frac{-\pi m_y}{d_{-1}}\right) = j \frac{k_{-1}^2 - k_{xm}^2}{k_0 \zeta_0 k_{zm,-1}} \cot(k_{zm,-1} h_{-1})$$
 (27)

where

$$k_{zm,-1} = \sqrt{k_{-1}^2 - k_{xm}^2 - (\pi m_y/d_{-1})^2}$$
 (28)

leading to

$$Y_{\text{down}}(k_{xm}) = \frac{-d_x}{d_{-1}} \sum_{m_y = -\infty}^{\infty} G_{xx}^{\text{cav}} \left(k_{xm}, \frac{-\pi m_y}{d_{-1}} \right) \times \text{sinc}^2 \left(\frac{\pi m_y d_1}{2d_{-1}} \right) C\left(m_y \right). \quad (29)$$

B. Medium Above the Feed

To find the expression for $Y_{up}(k_{xm})$, we first analyze the stratification above the PPW, which can be, for example, the dielectric slab shown in Fig. 11(a)

$$Y_{\text{strat}}(k_{xm}) = \frac{-d_x}{d_y} \sum_{m_y = -\infty}^{\infty} G_{xx}^{\text{strat}}(k_{xm}, k_{ym}) \operatorname{sinc}^2\left(\frac{k_{ym}d_1}{2}\right)$$
(30)

where $k_{xm} = k_{x0} - 2\pi m_x/d_x$ and $k_{ym} = k_{y0} - 2\pi m_y/d_y$, with $k_{x0} = k_0 \sin \theta \cos \phi$ and $k_{y0} = k_0 \sin \theta \sin \phi$, and ϕ is the azimuth scan angle. For a stratified dielectric medium, the spectral Green's function can be written in the form

$$G_{xx}^{\text{strat}}(k_{xm}, k_{ym}) = -\frac{1/Z_{\text{strat}}^{\text{TE}} k_{xm}^2 + 1/Z_{\text{strat}}^{\text{TM}} k_{ym}^2}{k_{xm}^2 + k_{ym}^2}$$
(31)

where $Z_{\text{strat}}^{\text{TM/TE}}$ refers to the input impedance of the transmission line representing the stratification for TE or TM mode.

For the general expression of $Y_{\rm up}(k_{xm})$, we assume that for every Floquet mode the PPW can be expressed as a transmission line section with characteristic impedance defined in (18) and propagation constant $k_{\rm z,1}=(k_1^2-k_{xm}^2)^{1/2}$. Thus, the admittance transfer formula can be used [13], resulting in

$$Y_{\text{up}}(k_{xm}) = \frac{1}{Z_1^{\text{PPW}}(k_{xm})} \frac{j \tan(k_{z,1}h_1)/Z_1^{\text{PPW}}(k_{xm}) + Y_{\text{strat}}(k_{xm})}{j \tan(k_{z,1}h_1)Y_{\text{strat}}(k_{ym}) + 1/Z_1^{\text{PPW}}(k_{ym})}.$$
(32)

C. Equivalent Circuit

Considering $Y_{\text{down}}(k_{x0})$ in (29), we can split this term into the fundamental mode ($m_y = 0$) and the higher order modes ($m_y \neq 0$). The latter contribution can be associated with the step capacitance. Therefore, at each step discontinuity, a shunt capacitance can be evaluated as follows:

$$Y_{\text{step}}^{\text{strat}} = \frac{-d_x}{d_{-1}} \sum_{m_y \neq 0} G_{xx}^{\text{strat}} (k_{x0}, k_{ym}) \operatorname{sinc}^2 \left(\frac{k_{ym} d_1}{2}\right)$$
(33)

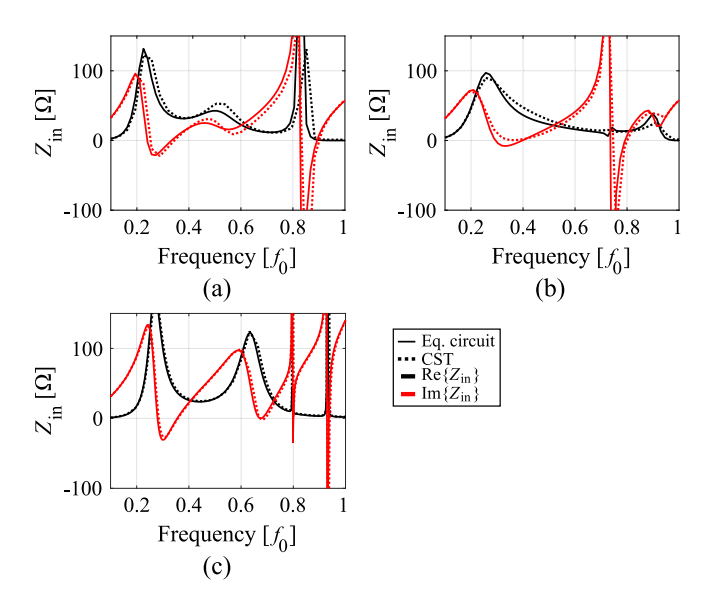


Fig. 12. Active input impedance of PPW-fed connected slot array when scanning to (a) $\theta=0^\circ$, (b) $\theta=60^\circ$ and $\phi=90^\circ$, and (c) $\theta=60^\circ$ and $\phi=0^\circ$. Unit cell parameters: $d_x=d_y=0.5\lambda_0,\ \delta=0.1\lambda,\ \varepsilon_{r,1}=\varepsilon_{r,-1}=1,\ \varepsilon_{r,2}=5,\ h_{-1}=0.1\lambda_0,\ h_1=0.2\lambda_0,\ h_2=0.25\lambda_0,\ d_{-1}=d_y,\ \text{and}\ d_1=0.1\lambda_0.$

$$Y_{\text{step}}^{\text{feed}} = \frac{-d_x}{d_{-1}} \sum_{m_y \neq 0} G_{xx}^{\text{cav}} \left(k_{x0}, \frac{-\pi m_y}{d_{-1}} \right) \text{sinc}^2 \left(\frac{\pi m_y d_1}{2d_{-1}} \right) C(m_y)$$
(34)

for the steps at the open end of the PPW and at the feed, respectively.

The fundamental mode $m_y = 0$ can be represented as the equivalent circuit model in Fig. 11(b), where each PPW is described as a transmission line section with characteristic impedance $Z_{c,1}^{\rm PPW}$ and $Z_{c,-1}^{\rm PPW}$ for the PPW and the cavity, respectively. The stratified medium in which the array radiates is represented as a pair of transmission lines, for TE and TM modes, respectively, connected by transformers $\sin \phi$ and $\cos \phi$, as done in [15]. A transformer with turn ratio $n_{\rm strat} = (d_x/d_y)^{0.5} \times {\rm sinc}(k_{y0}d_1/2)$ is included to account for the aspect ratio of the unit cell dimensions and the scanning in the E-plane. It can be noted that the provided transmission line model represents in the same circuit both the guided mode inside the PPW and the radiated mode in free space.

D. Validation of the Circuit

To validate the model, a comparison between the proposed equivalent circuit and CST is given in Fig. 12. This considers a connected PPW array, backed by a cavity, and loaded with a dielectric slab of relative permittivity $\varepsilon_{r,2} = 5$ and thickness $h_2 = 0.25\lambda_0$. The slab is sized so that surface waves occur within the frequency range of investigation, to validate the model also for the estimation of resonances.

It can be seen that there is a good correspondence between the analytical method and the full-wave simulation, both for broadside [Fig. 12(a)] and scanning to $\theta = 60^{\circ}$ in the E-plane [Fig. 12(b)].

With the equivalent circuit representation, more complex superstrates including ADLs that are optimized for wideband performance can also be analyzed and designed. One such

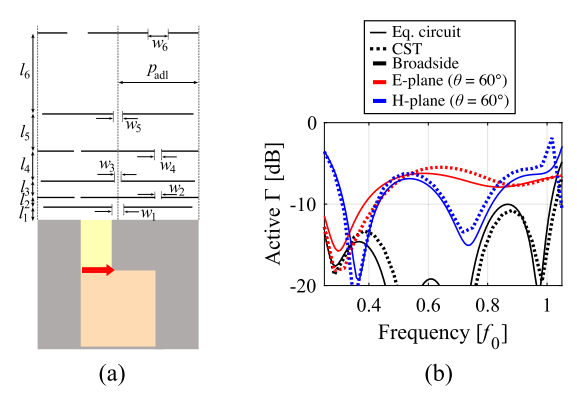


Fig. 13. (a) Side view of the wideband array unit cell and (b) active reflection coefficient computed with the analytical model and using CST. Unit cell parameters: $d_x = d_y = 0.445\lambda_0$, $\delta = 0.13\lambda_0$, $\varepsilon_{r,1} = 1.7$, $\varepsilon_{r,-1} = 1.5$, $d_1 = 0.085\lambda_0$, $d_{-1} = 0.2\lambda_0$, $h_1 = 0.14\lambda_0$, and $h_{-1} = 0.22\lambda_0$. ADL parameters: $p_{\text{ADL}} = d_x/2$, $w_1 = 0.034\lambda_0$, $w_2 = 0.017\lambda_0$, $w_3 = 0.020\lambda_0$, $w_4 = 0.019\lambda_0$, $w_5 = 0.028\lambda_0$, $w_6 = 0.056\lambda_0$, $l_1 = 0.034\lambda_0$, $l_2 = 0.026\lambda_0$, $l_3 = 0.045\lambda_0$, $l_4 = 0.082\lambda_0$, $l_5 = 0.102\lambda_0$, and $l_6 = 0.221\lambda_0$. The interlayer shifts are maximum.

example is given in Fig. 13(a), where the array is loaded with a six-layer ADL. The ADLs are modeled in the transmission line representing the stratification above the PPW using the method developed in [8]. Compared with the CST simulation (dashed line), a fair agreement can be observed in the estimation of the active reflection coefficient, as shown in Fig. 13(b), for broadside and scanning in the main planes to 60°. The difference between our method and CST is in line with previous results of the connected array with artificial dielectrics in [6] and [7] and can be attributed to the approximation used for the current distribution on the array aperture, that might be affected by the lowest patch layer.

VI. MULTIPLE PPW SECTIONS

The procedure explained in Section V rigorously describes a method to obtain Z_{in} for a connected array consisting of a single PPW section, a stratified medium, and a cavity.

In the case of multiple PPW sections of finite length, the expression of the step capacitance at every discontinuity cannot be found in a rigorous manner, since we are neglecting the interaction of higher order modes $m_y \neq 0$ between the two ends of a PPW section. Nevertheless, we can approximate the step capacitance at each discontinuity as the one derived for the infinitely long PPWs in (25). This approximation is based on the assumption that the reactive energy due to the fringing field is localized near the discontinuity and does not change with the PPW length.

By computing the input admittance above and below the feed, the total active input impedance can be found using (26).

A. Multisection PPW Validation

To validate the multisection PPW model, the structure in the inset of Fig. 14 is considered, consisting of a cavity below the feed and three PPW sections with equal length h. The PPWs are filled with free space and mutually shifted such that they have one common wall.

When finite PPW sections are used, the real part of the impedance is no longer frequency independent as shown in

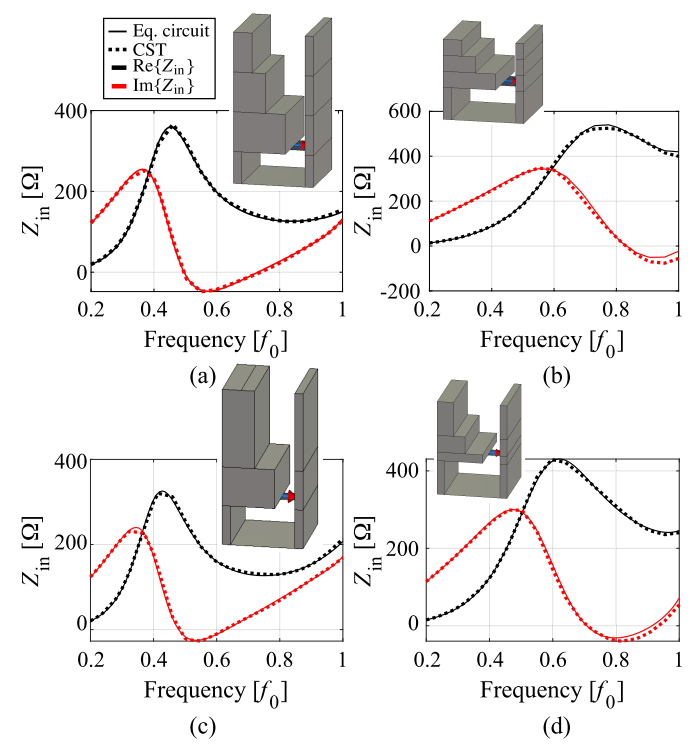


Fig. 14. Comparison of multisection PPW array between CST and equivalent circuit when scanning to $\theta=60^\circ$ and $\phi=0^\circ$, with dimensions $d_x=d_y=\lambda_0/2,\, d_{-1}=\lambda_0/2.5,\, d_1=\lambda_0/8,\, d_2=\lambda_0/4,\, d_3=\lambda_0/3,\, \delta=d_x/4,\, \epsilon_{r,1}=\epsilon_{r,2}=\epsilon_{r,3}=1,\, \text{and}\,\, h_{-1}=\lambda_0/4,\, \text{for}\,\, (a)\,\, h_1=h_2=h_3=\lambda_0/4,\, (b)\,\, h_1=h_2=h_3=\lambda_0/20,\, (c)\,\, h_1=\lambda_0/4,\, h_2=\lambda_0/2,\, \text{and}\,\, h_3=0,\, \text{and}\,\, (d)\,\, h_1=\lambda_0/16,\, h_2=\lambda_0/8,\, \text{and}\,\, h_3=\lambda_0/4.$

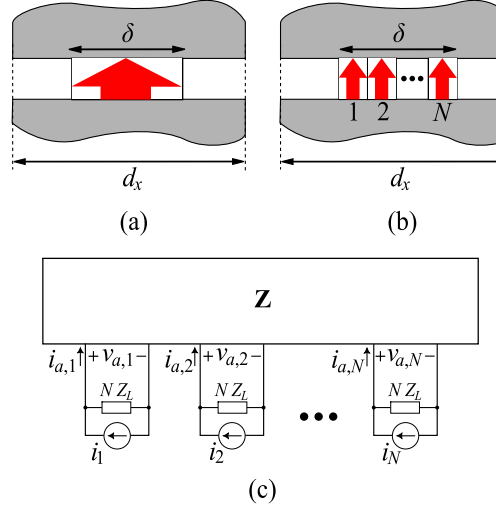


Fig. 15. (a) Schematic of slot/PPW with electrically large δ -gap feed. (b) Feed is split in N smaller size feeds. (c) Circuit representation of the N feeds.

Fig. 6, but it varies as a function of frequency. The impedance values are much higher than the infinite PPW case since the free space impedance (377 Ω) is transferred by a line section with a finite length. The typical oscillations with frequency due to impedance transfer can be observed. Moreover, the presence of the cavity below the feed results in a low input resistance and inductive reactance at the lower frequencies.

A comparison with CST is shown for two different lengths of the PPWs, namely, $\lambda_0/4$ and $\lambda_0/20$. A good comparison can be observed for the longer PPW [Fig. 14(a)], but the approximation seems to remain accurate also for the shorter

PPWs [Fig. 14(b)]. To demonstrate the generic applicability of the model, also two cases with unequal PPW section lengths are shown to agree well with CST simulations in Fig. 14(c) and (d).

VII. CONCLUSION

A spectral domain method was presented for the analysis of PPW-fed connected slot arrays. The method allows to derive the closed-form expressions to estimate the active input impedance of the array with negligible computational resources.

An equivalent circuit of the unit cell was also derived, where the PPWs sections are represented in terms of equivalent transmission lines, and closed-form expressions are given for the capacitance associated with step discontinuities of the PPW and the inductance associated with the feed. The model can be used for several geometries including PPW in general stratified media and multisection PPWs with nonaligned axes.

The model was validated by comparing the analytical input impedance with full-wave simulations and a good correspondence between both methods was observed. The method can be used for the design of wideband PPW-fed connected arrays, enabling the optimization of the unit cell performance including the feed.

$\begin{array}{c} \text{Appendix} \\ \text{Improved Analysis of Large δ-Gap Feeds for} \\ \text{H-Plane Scanning} \end{array}$

The analysis of connected arrays is valid for electrically small δ -gap feed sizes [12]. For broadside radiation or when scanning in the E-plane, the voltage over the feed is approximately constant, and the model remains accurate for electrically large δ -gap sizes. However, when scanning in the H-plane, the voltage can vary along the feed length. Therefore, the approximation of constant voltage and current in the gap is no longer valid.

To improve the accuracy of the input impedance calculation for H-plane scanning, we introduce an extension of the method presented in this article. The proposed approach involves splitting the large feed [Fig. 15(a)] into N smaller subfeeds, each with size δ/N [Fig. 15(b)]. The number N can be chosen such that the size of each individual subfeed is $\approx \lambda_0/10$. The center of the nth feed is defined as follows:

$$x_n = \frac{\delta}{2} \left(\frac{2n-1}{N} - 1 \right). \tag{35}$$

The combination of the multiple feeds can be represented as the N-port network in Fig. 15(c), where the **Z** represent the impedance matrix whose entries are defined as follows:

$$Z_{mn} = -\frac{1}{d_x} \sum_{m_x = -\infty}^{\infty} \frac{\operatorname{sinc}^2(\frac{k_x m \delta}{2N}) e^{-jk_{xm}(x_n - x_m)}}{D_1(k_{xm}) + D_{-1}(k_{xm})}.$$
 (36)

We define the vector of the incident currents as a column vector with N elements equal to $i_n = I_0$. Assuming that the original large feed has an internal impedance Z_L , the internal impedance of the subfeeds can be represented as an $N \times N$ matrix

$$\mathbf{Z}_L = Z_L N \mathbf{I_N} \tag{37}$$

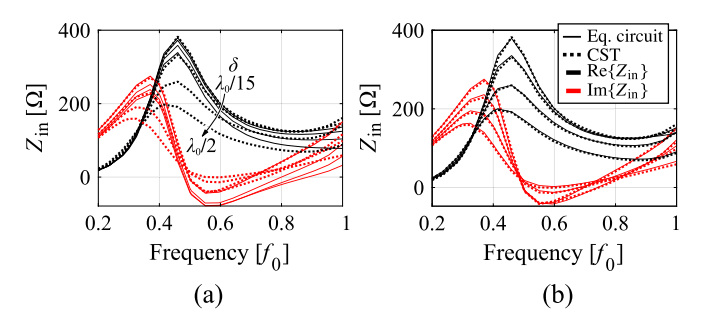


Fig. 16. Comparison of active input impedance scanning to $\theta=60^\circ$ in the H-plane, for different δ values. (a) With the conventional single feed and (b) using up to N=5 subfeeds for the largest value of δ . The geometry of Fig. 14 is used.

where I_N is the identity matrix of size N. By computing the parallel of the input impedance \mathbf{Z} and the reference impedance \mathbf{Z}_L in matrix form, and multiplying it with the incident currents, the active voltages can be computed as follows:

$$\mathbf{v}_a = (\mathbf{Z} + \mathbf{Z}_L)^{-1} \mathbf{Z}_L \mathbf{Z} \mathbf{i}. \tag{38}$$

From the active voltage, the active current is found as follows:

$$\mathbf{i}_a = \mathbf{Z}^{-1} \mathbf{v}_a. \tag{39}$$

Since the subfeeds are in parallel, we can define the active input impedance of the combined feed as the ratio between the average active voltage and the total current over the δ -gap

$$Z_{\rm in} = \frac{\frac{1}{N} \sum_{n=1}^{N} v_{a,n}}{\sum_{n=1}^{N} i_{a,n}}.$$
 (40)

For comparison, the multisection PPW geometry reported in Fig. 14 was analyzed for $\delta \in [\lambda_0/15, \lambda_0/2]$ using the conventional single feed in Fig. 16(a) and up to N=5 subfeeds in Fig. 16(b), both for scanning to $\theta=60^\circ$. It is evident that the use of multiple subfeeds, allowing for the variation of voltage and current within the feed, yields a more accurate estimation of the input impedance.

REFERENCES

- [1] J. J. Lee, S. Livingston, R. Koenig, D. Nagata, and L. L. Lai, "Compact light weight UHF arrays using long slot apertures," *IEEE Trans. Antennas Propag.*, vol. 54, no. 7, pp. 2009–2015, Jul. 2006.
- [2] S. S. Holland and M. N. Vouvakis, "The planar ultrawideband modular antenna (PUMA) array," *IEEE Trans. Antennas Propag.*, vol. 60, no. 1, pp. 130–140, Jan. 2012.
- [3] R. W. Kindt and W. R. Pickles, "Ultrawideband all-metal flared-notch array radiator," *IEEE Trans. Antennas Propag.*, vol. 58, no. 11, pp. 3568–3575, Nov. 2010.
- [4] D. H. Schaubert, S. Kasturi, A. O. Boryssenko, and W. M. Elsallal, "Vivaldi antenna arrays for wide bandwidth and electronic scanning," in *Proc. 2nd Eur. Conf. Antennas Propag. (EuCAP)*, Edinburgh, U.K., Nov. 2007, pp. 1–6.
- [5] M. Cooley et al., "Planar-fed folded notch (PFFN) arrays: A novel wideband technology for multi-function active electronically scanning arrays (AESAs)," in *Proc. IEEE Int. Symp. Phased Array Syst. Technol.* (PAST), Waltham, MA, USA, Oct. 2016, pp. 1–6.
- [6] W. H. Syed, D. Cavallo, H. Thippur Shivamurthy, and A. Neto, "Wideband, wide-scan planar array of connected slots loaded with artificial dielectric superstrates," *IEEE Trans. Antennas Propag.*, vol. 64, no. 2, pp. 543–553, Feb. 2016.
- [7] R. Ozzola, A. Neto, U. Imberg, and D. Cavallo, "Connected slot array with interchangeable ADL radome for sub-8 GHz 5G applications," *IEEE Trans. Antennas Propag.*, vol. 72, no. 1, pp. 992–997, Jan. 2024.

- [8] D. Cavallo and R. M. van Schelven, "Closed-form analysis of artificial dielectric layers with non-periodic characteristics," in *Proc. 13th Eur. Conf. Antennas Propag. (EuCAP)*, Krakow, Poland, Mar. 2019, pp. 1–5.
- [9] D. Cavallo, "Parallel-plate waveguide-feeding structure for planarconnected arrays," *IEEE Antennas Wireless Propag. Lett.*, vol. 21, no. 4, pp. 765–768, Apr. 2022.
- [10] F. F. Manzillo, M. Ettorre, M. Casaletti, N. Capet, and R. Sauleau, "Active impedance of infinite parallel-fed continuous transverse stub arrays," *IEEE Trans. Antennas Propag.*, vol. 63, no. 7, pp. 3291–3297, Jul. 2015.
- [11] M. Del Mastro et al., "Analysis of circularly polarized CTS arrays," *IEEE Trans. Antennas Propag.*, vol. 68, no. 6, pp. 4571–4582, Jun. 2020.
- [12] D. Cavallo, "Connected array antennas: Analysis and design," Ph.D. dissertation, Tech. Univ. Eindhoven, Eindhoven, The Netherlands, Nov. 2011.
- [13] D. M. Pozar, Microwave Engineering, 4th ed. Hoboken, NJ, USA: Wiley, 2012.
- [14] N. Marcuvitz, Waveguide Handbook, Piscataway, NJ, USA: IEEE Press, 1986
- [15] D. Cavallo, A. Neto, and G. Gerini, "Green's function based equivalent circuits for connected arrays in transmission and in reception," *IEEE Trans. Antennas Propag.*, vol. 59, no. 5, pp. 1535–1545, May 2011.



Caspar M. Coco Martin (Graduate Student Member, IEEE) received the M.Sc. degree (cum laude) in electrical engineering from Delft University of Technology (TU Delft), Delft, The Netherlands, in 2022, where he is currently pursuing the Ph.D. degree with the Terahertz Sensing Group.

His research interests include wideband arrays, metamaterials, and (semi-) analytical electromagnetic analysis methods.

Mr. Coco Martin was a recipient of the Excellent Presentation Award at the IEEE Ukrainian

Microwave Week in 2022 and the Best Antenna Theory Paper Award at the 18th European Conference on Antennas and Propagation (EuCAP) in 2024.



Daniele Cavallo (Senior Member, IEEE) received the M.Sc. degree (summa cum laude) in telecommunication engineering from the University of Sannio, Benevento, Italy, in 2007, and the Ph.D. degree (cum laude) in electromagnetics from Eindhoven University of Technology, Eindhoven, The Netherlands, in 2011.

From 2007 to 2011, he was with the Antenna Group, Netherlands Organization for Applied Scientific Research, The Hague, The Netherlands. From 2012 to 2015, he was a Post-Doctoral

Researcher with the Microelectronics Department, Delft University of Technology (TU Delft), Delft, The Netherlands. In 2015, he joined the Chalmers University of Technology, Gothenburg, Sweden, as a Visiting Researcher. He is currently an Associate Professor with the Terahertz Sensing Group, TU Delft. He has authored or co-authored about 200 papers published in peer-reviewed international journals and conference proceedings. His current research interests include wideband antenna arrays, analytical and numerical methods for antenna characterization, and millimeter-wave integrated antennas.

Dr. Cavallo was a recipient of the Best Innovative Paper Prize at the European Space Agency Antenna Workshop in 2008, the Best Paper Award in Electromagnetics and Antenna Theory at the 11th European Conference on Antennas and Propagation (EuCAP) in 2017, and the Best Antenna Theory Paper Award at EuCAP 2024. He received the "Veni" Personal Grant from the Netherlands Organization for Scientific Research in 2015. His students received the Best Student Paper Award at EuCAP in 2013, the Else Kooi Prize in 2016, and the Excellent Presentation Award at the IEEE Ukrainian Microwave Conference in 2022. He is the Co-Coordinator of the EurAAP working group "Active Array Antennas." He has served as an Associate Editor for IEEE TRANSACTIONS ON ANTENNAS AND PROPAGATION from 2016 to 2023. He was a Thematic TPC Chair of Antennas and Electromagnetics at EuCAP 2024, Glasgow, U.K.